John von Neumann Institute for Computing

Structural, Electronic, and Optical Properties of Semiconductor Nanocrystallites

L. E. Ramos, F. Bechstedt

published in

NIC Symposium 2008,
G. Münster, D. Wolf, M. Kremer (Editors),
John von Neumann Institute for Computing, Jülich,
NIC Series, Vol. **39**, ISBN 978-3-9810843-5-1, pp. 185-192, 2008.

http://www.fz-juelich.de/nic-series/volume39

Structural, Electronic, and Optical Properties of Semiconductor Nanocrystallites

Luis E. Ramos and Friedhelm Bechstedt

Friedrich-Schiller-Universität Jena, Institut für Festkörpertheorie und -optik
Max-Wien-Platz 1, D-07743 Jena, Germany
E-mail: lramosde@yahoo.de,bechstedt@ifto.physik.uni-jena.de

We investigate the electronic and optical properties of large Si and Ge nanocrystallites by means of an *ab initio* pseudopotential method based on density-functional theory and on the GW approximation (Green function and screened Coulomb potential). The nanocrystallites studied may contain more than four hundred atoms and more than one thousand electrons. We find important effects of the oxidation, oxide capping, germanium (silicon) capping, and different surface terminations, and doping (group III, group-IV, and group-V impurities) on the electronic structure and optical absorption spectra are studied semiconductor nanocrystallites.

1 Introduction and Motivation

Silicon nanocrystallites (NCs) have been intensively investigated in the last years due to their interesting quantum confinement properties.[1] The strong spatial localization of electrons and holes in Si NCs can enhance radiative recombination rates and give rise to luminescence. Among other known applications, research on Si NCs could lead to optoelectronic devices compatible with the consolidated Si technology. Optical gain in Si NCs has been reported,[3] and new devices have recently been suggested.[4] The most accepted models to explain the PL in nanosized materials are related to quantum confinement effects.

The role of oxygen in the peak position and efficiency of the PL has been demonstrated for oxidized Si NCs.[5] While the PL blue shift from Si NCs embedded in SiO_2 matrices and from the oxidation of porous Si seems to support the quantum confinement model, there is evidence that a PL red shift is caused by defect states.[5] Our calculations consider some Si NCs whose surface is completely oxidized,[6,7] which can explain better the variation of properties of nanometer-sized Si dots with backbond oxidation in comparison to those for H and OH passivations.[8]

Electrical and mechanical properties resulting from the combination of group-IV compounds such as Si and Ge indicate that their heterostructures and nanostructures are very promising materials in device technology.[9] Direct applications of the SiGe technology comprehend high-frequency transistors, infrared photodetectors and photodiodes, and solar cells. Besides new features in the electronic properties, SiGe-based NCs can provide different quantum confinement for carriers and charge-storage mechanisms, the latter being useful for low-power memory devices.

The influence of doping on the electronic properties observed in porous Si (pSi) composed by Si NCs of different sizes is still being investigated.[10] Doping of Si NCs is expected to introduce additional levels close to the HOMO (the highest occupied molecular orbital) or LUMO (lowest unoccupied molecular orbital) in the same fashion as it does for Si bulk. This fact could enhance the intensity of absorption and emission spectra and be useful in some applications.

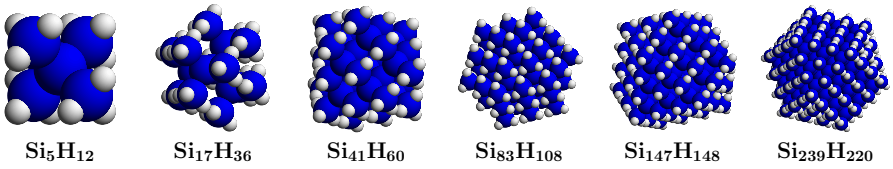

Figure 1. Faceted semiconductor nanocrystallites studied. The dark spheres correspond to Si or Ge atoms and the light ones to H atoms.

In order to model Si (Ge) NCs with a reasonable size and oxidation of Si NCs, a considerable computational power is needed, since a large number of electronic states is involved. In the following we describe the main results obtained for oxidation, capping, and doping of Si NCs. In Sec. 2 we describe the methods and approaches used in the calculations. The results are presented in Sec. 3 and in Sec. 4 we summarize our main results and conclusions.

2 Methods

We employ the density-functional theory (DFT), local-density approximation (LDA) or generalized-gradient approximation (GGA), as implemented in the Vienna *Ab initio* Simulation Package (VASP).[11,12] Projector-augmented-wave (PAW) data sets are applied to treat the interaction of electrons with the nuclei analogously to the pseudopotential method. The eigenfunctions and eigenvalues of the many-electron system are determined by solving the Kohn-Sham (KS) equations. The PAW data sets are suitable to calculate optical matrix elements with good accuracy.[13] VASP uses a plane-wave basis, the supercell approximation in the reciprocal space, and iterative matrix-diagonalization schemes, which are based on optimized minimization algorithms such as conjugate-gradient method, residual band-by-band minimization, and block Davidson.[14] The energy cutoffs required for the planewave basis are relatively low, which allows us to treat efficiently systems with hundreds of atoms. VASP requires standard linear-algebra libraries such as LAPACK (Linear Algebra PACKage) and BLAS (Basic Linear Algebra Subprograms),[15] but others such as ESSL (Engineering Scientific Subroutine Library), ScaLAPACK (Scalable LAPACK), ATLAS (Automatically Tuned Linear Algebra Software)[16] can also be used. The algorithms implemented in VASP allow several parts of the code to be parallelized using MPI (Message Passing Interface), e.g. parallelization over electronic bands and planewave coefficients.

The NCs have a shell-like structure and lie in large simple-cubic supercells. Starting from a central Si atom and assuming tetrahedral coordination, the NCs are constructed by adding the neighbouring atoms shell by shell. The dangling bonds at the NC surface are passivated with H atoms. In the case of doping, we consider additional Si NCs with a spherical-like shape. The faceted NCs investigated are shown in Fig. 1. To simplify the description of the NCs, in the following we denote them according to the number of atom shells in their core and in their capping shells: Si_5H_{12}, $Si_{17}H_{36}$, $Si_{41}H_{60}$, $Si_{83}H_{108}$, $Si_{147}H_{148}$, and $Si_{239}H_{220}$ are respectively Si2, Si3, Si4, Si5, Si6, and Si7. Oxidation in Si NCs is considered via the passivation of the dangling bonds with hydroxyls (OH) or as a

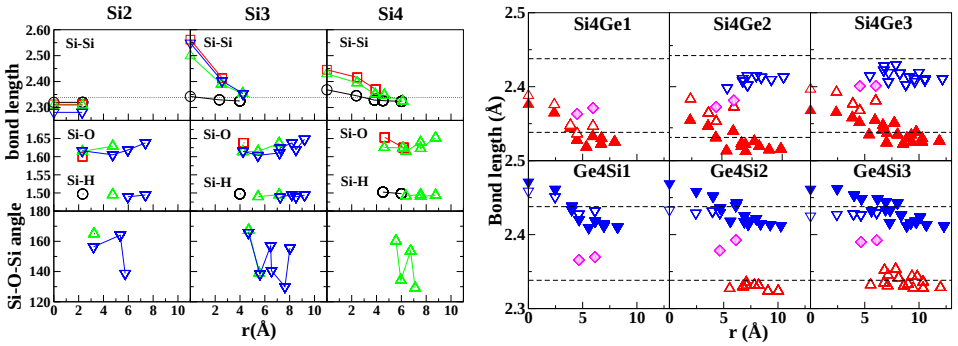

Figure 2. Left: Average bond lengths (in Å) and Si-O-Si angles (in degrees) versus distance from centre of the NCs for Si cores with varying size. The different oxidation stages are indicated by circles (H passivation), squares (OH passivation), up triangles (one oxide shell), and down triangles (two oxide shells). The dotted lines indicate the bulk Si bond length. Right: Si-Si bond lengths (up triangles), Ge-Ge bond lengths (down triangles), and Si-Ge bond lengths (diamonds) versus distance of the atom from the centre of the NC for the Ge-capped Si NCs (upper panels) and for the Si-capped Ge NCs (lower panels). The Si-Si bulk bond length (2.34 Å) and the Ge-Ge bulk bond length (2.44 Å) are indicated by the dashed lines. The filled triangles correspond to the Si and Ge NCs passivated with H and with the same number of shells as the capped Si (Ge) NCs in each frame.

backbond oxidation of one and two shells immediately below the surface.[7] To achieve a total energy minimum and negligible interatomic forces, we perform the ionic relaxation for all NCs without symmetry constraint. Spin polarization is taken into account in the case of doped Si NCs.

The optical matrix elements are calculated within the framework of the independent-particle approximation (DFT/KS) or independent-quasiparticle approximation (GW). The optical absorption spectra are identified as the imaginary part of the corresponding dielectric function and a Lorentzian broadening of 0.1 eV is applied in all spectra.

3 Results

3.1 Structural Properties

In Fig. 2 we summarize the structural properties of oxidized Si NCs and Si (Ge) capped NCs after ionic relaxation. As a result of ionic relaxation, the Si-Si bond lengths in the oxidized Si NCs deviate from the bulk value differently in the core and close to the surface of the NCs. The Si-Si bond lengths of very small Si NCs are slightly shortened with respect to the bulk value, whereas the largest cores Si3 and Si4 exhibit an expansion of the Si-Si bonds at the core. Oxidation of the Si NCs increases the expansion of the Si-Si bonds. The Si-O bonds lengths increase slightly close to the outermost shells of the NC, while the Si-H bond lengths practically do not vary versus the NC radii. As a result of the relaxation, the Si-O-Si angles tend to decrease versus the distance from the centre of the Si NC.[7]

Si and Ge NCs passivated with H also exhibit an expansion of the Si-Si or Ge-Ge bond lengths with respect to their bulk value at the centre of the NC and a contraction of the same bonds near the surface.[7] For the Ge-capped Si NCs, the Si-Si bonds lengths follow

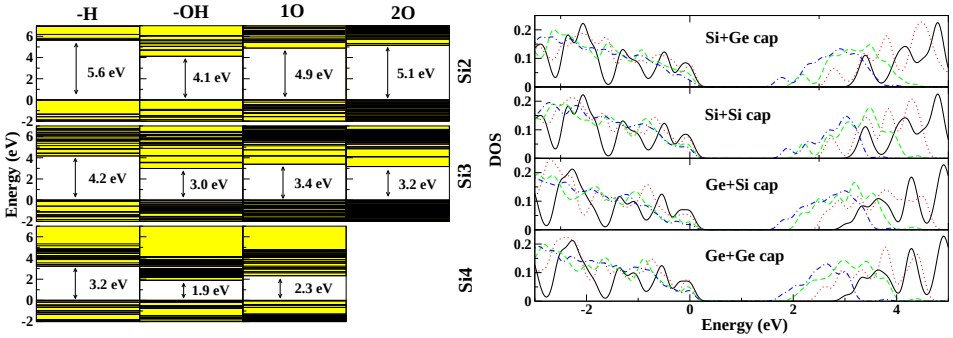

Figure 3. Left: Electronic levels of the Si NCs with different passivation and oxide coverage as calculated by DFT-LDA. In the columns, from the left to the right, the electronic levels for NCs passivated with H, passivated with OH, with one covering oxide shell, and with two covering oxide shells. The number of Si atoms in the core of the NCs is indicated at the right side. The values of the HOMO-LUMO gaps are indicated by the arrows. Right: Density of states for capped and uncapped NCs with 4 shells (solid lines, uncapped NC), 5 shells (dotted lines), 6 shells (dashed lines), and 7 shells (dot-dashed lines). The HOMO of all the structures is aligned to the energy zero.

the same trend as for the Si NCs. The Ge-Ge bond lengths in the capping shells are smaller than the one for Ge bulk and tend to have similar values with increasing number of capping shells. However, for the Si-capped Ge NCs there is a tendency for both Ge-Ge and Si-Si bond lengths to be slightly smaller than their corresponding bulk values and to vary much less than for the Ge NCs. The Si-Ge bonds at the interface between the capping shell and the NC core increase with an increasing size of the NC in both Si-capped and Ge-capped structures. The Si-Si and Ge-Ge bond lengths in the Si-capped Ge NCs indicate a small strain of the bonds which is even lower than the one for Ge NCs.

3.2 Electronic Properties

The effect of oxide coverage on the DFT-LDA KS eigenvalues of Si NCs is shown in Fig. 3. Both the passivation of the Si NC with OH and the oxide coverage give rise to a narrowing of the HOMO-LUMO energy gap. The narrowing of the gap is more pronounced in the case of passivation with OH than in the case of an oxide coverage of the Si NCs. As the size of the Si NC core increases, the HOMO-LUMO gap narrows as a consequence of the reduced spatial confinement of the corresponding states. In Fig. 3, we show the effect of the capping shells in Ge and Si NCs on the electronic density of states (DOS). As a rule, the increasing size of the NCs leads to a reduction of the quantum confinement and the HOMO-LUMO energy gap narrows. As shown in Fig. 3, the structures that contain more Ge atoms tend to have a narrower gap than the structures which contain more Si atoms. In this sense, our well-ordered capped NCs can be considered as one of the possible configurations of a SiGe random-alloy nanocrystallite. One can therefore identify two competing effects in determining the HOMO-LUMO gap of the capped Si and Ge NCs. One is due to quantum confinement and the other one is dictated by the overall composition of the NC. The reduction of quantum confinement combined with the increase of Ge contents is very effective in shortening the HOMO-LUMO gap of the Ge-capped Si NCs.

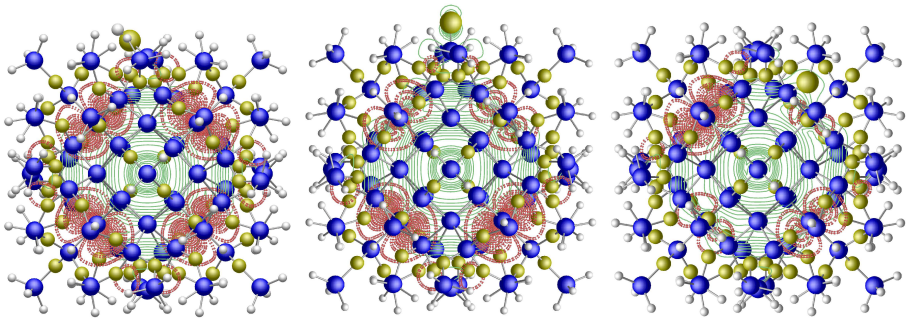

Figure 4. From the left to the right we show optimized structures for the single terminations -OH and =O, and the oxygen vacancy in the oxidized NC Si4-1O. The dashed red lines indicate the charge distribution of HOMO and the solid green lines indicate the charge distribution of the LUMO. The Si (blue spheres), O (yellow spheres), and H (white spheres) atoms in the Si NC are represented. The largest spheres in each picture correspond to the termination or site where the defect is localized.

3.3 Defects and Doping of Si Nanocrystallites

In Fig. 4 we show the effect of a modified surface termination and the presence of defects in oxidized Si NC. The model system is a Si NC with one oxide shell and passivated with H (Si4-1O). In order to study the effect of oxygen-related defects on Si NCs, we consider an oxygen vacancy V_O in a Si-O-Si bond, a OH replacing a H atom, and a double-bonded oxygen atom replacing two H atoms (Si=O) at the surface of an oxidized NC.[6] The V_O is introduced in a Si-O-Si bond, whereas the -OH and =O defects are located at the central atom of a facet. Practically no influence on the electronic structure (not shown) is observed when a H atom is replaced by a OH group. Slight changes occur for the probability distributions of HOMO and LUMO according to Fig. 4. While the HOMO is mostly localized at the interface between the core and the oxide shell of the NCs, the LUMO is delocalized and spreads over the whole NC extent.[6] Although the influence in the case of the =O and V_O defects is more pronounced than that of the -OH defect, the regions where the HOMO and LUMO are localized remain the same as for the case of the defect-free oxidized Si NC.

The formation energies of group-III (B and Al), group-IV (C and Ge), and group-V (N and P) impurities versus the reciprocal radii of the Si NCs are shown in Fig. 5 and calculated by $\Omega_{\rm f}[X] = E_{\rm tot}[X] - E_{\rm tot} + \mu_{\rm Si} - \mu_X$, where $E_{\rm tot}[X]$ (X=B, Al, C, Ge, N, and P) is the total energy of the doped Si NC, $E_{\rm tot}$ is the total energy of the undoped Si NC, and $\mu_{\rm Si}$ and μ_X are estimates for the chemical potentials of the reservoirs for the Si and for the X species, respectively.[10] The influence of shape and size of the NCs on the impurity formation energies is shown in Fig. 5 for doped Si NCs versus their reciprocal radii. The formation energies of Ge and P impurities depend mainly on the size of the particle and have an almost linear dependence on the reciprocal radius of the Si NC. While the formation energy of the first-row elements C and N may increase for large Si NCs, the formation energy of B, Al and P decreases. Since B leads to symmetry lowering as Al does and large deformation as P does, the impurity formation energies of B are high in small Si NCs. Only the formation energy of the Ge impurity is nearly independent of the size of the nanocrystallite. This fact is related to the similar chemical properties of Si and

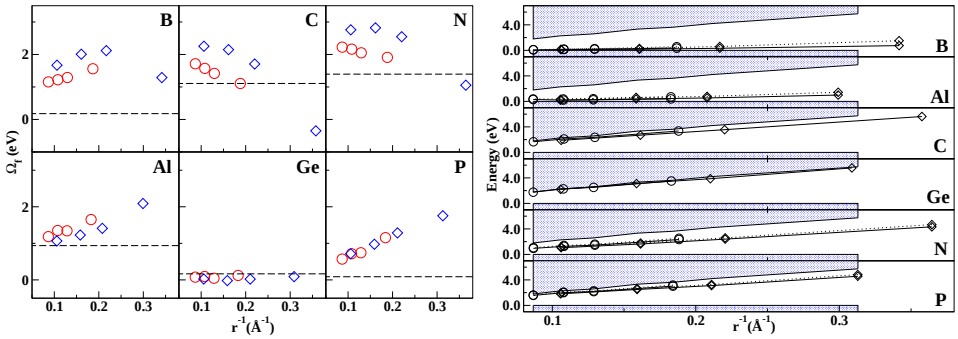

Figure 5. Left: Impurity formation energies of B, Al, C, Ge, N, and P versus the reciprocal radii of the doped Si NCs. The energy values are given for faceted (diamonds, see Fig. 1) and spherical-like (circles) doped Si NCs. The dashed lines indicate the impurity formation energies in bulk Si. Right: Energetic position of the KS impurity levels versus the reciprocal radii of the spherical-like (circles) and faceted (diamonds) Si NCs. The solid and dotted lines correspond to the spin-up and spin-down impurity levels. For the C- and Ge-doped Si NCs, the position of the LUMO is shown instead of the impurity level.

Ge. A comparison between faceted and spherical-like NCs shows that the incorporation of the impurity in Si NCs is more favourable, if the NC has facets in the case of Al, nearly shape-independent for Ge and P, and costs more energy for the other impurities considered. Except for Ge and the C and N doping of the smallest Si NCs, the impurity formation energies of the Si NCs are higher than in Si bulk. This can be explained in terms of longer Si-X bond lengths and the symmetry lowering of the doped Si NCs, which require additional relaxation of the atomic positions in comparison with bulk Si.

In Fig. 5 the position of the KS impurity levels in the energy-gap region as well as the HOMO-LUMO gap of the undoped Si NCs shows nearly a linear dependence versus the reciprocal radii of the NCs. An increase of quantum confinement leads to deep impurity levels in the doped Si NCs. In Si NCs the B and Al impurities induce shallow acceptor levels, whereas the N and P impurities induce deep and shallow donor levels, respectively. Only small variations of the HOMO-LUMO gaps due to the shape of the Si NCs can be perceived in figure 5 and do not vary significantly with the shape of the Si NCs.

3.4 Optical Absorption Spectra

In Fig. 6, the optical absorption spectra within the independent-quasiparticle approximation (GW) and HOMO-LUMO gaps are presented for different Si NC core sizes, passivations, and capping oxide shells. Si NCs passivated with hydroxyls have a more pronounced narrowing of the gap than the ones with an oxide coverage and the ones passivated with H. The most intense optical transitions occur at higher energies than the HOMO-LUMO gap and tend to increase with increasing oxygen contents and increasing size of the Si NCs. The indirect-gap character of bulk Si is transferred to all defect-free Si NCs independently of how oxygen is incorporated, via passivation with OH or via backbond oxidation. Our results indicate that the main influence of oxygen on the optical properties of defect-free Si NCs are the shifts of onset of the absorption in the case of the backbond oxidation and

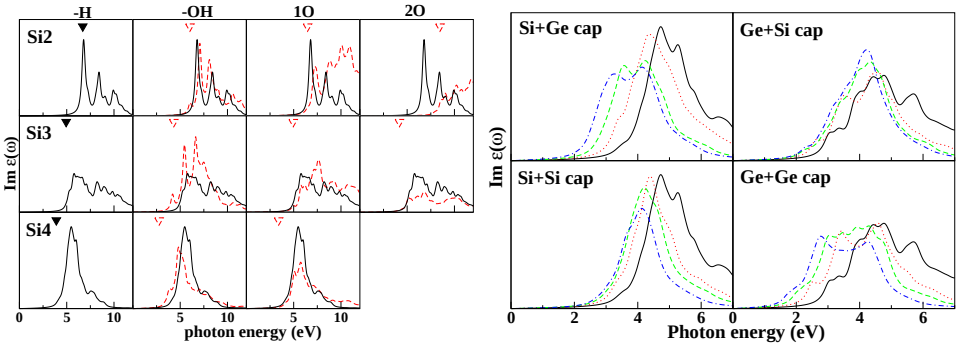

Figure 6. Left: Optical absorption spectra (arbitrary units) within the independent-quasiparticle approximation for Si NCs passivated with H (solid lines), passivated with OH, with one oxide shell 1O, and with two oxide shells 2O (columns), (dashed lines) and for Si2, Si3, and Si4 cores (rows). The HOMO-LUMO gaps are indicated by triangles (solid/dashed). Right: Optical absorption spectra of NCs with Si core (left panels) and NCs with Ge core (right panels). The upper panels correspond to the capped structures, whereas the lower panels show the spectra of Si and Ge NCs. For Si4(Ge4) NC core the spectra are shown for the case without capping shells (solid lines), one (dotted lines), two (dashed lines), and three (dot-dashed lines) capping shells.

passivation with OH. Backbond oxidation blue shifts the onsets of absorption of Si NCs with oxygen contents of bulk Si. The larger the Si NCs with backbond oxidation are, the smaller are the relative blue shifts of the onsets of absorption.

In Fig. 6, we present the optical absorption spectra of the capped and uncapped Si(Ge) NCs. As for the DOS in Fig. 3, the absorption spectra in Fig. 6 show clearly the importance of quantum confinement in determining the HOMO-LUMO gap. The addition of Ge capping shells to both Si and Ge NCs shifts the peaks of the absorption to red. Conversely to what is depicted from Fig. 3, the absorption spectra of the Si-capped Ge NCs shows a compensation effect between the composition of the NCs and their quantum confinement properties given by their size. In the Si-capped Ge NCs the addition of Si atoms tends to increase the value of the HOMO-LUMO gap due to the composition, whereas the increasing number of shells and consequently the size of the NC tends to reduce its value. As a result, the absorption peaks are not so shifted to red as in the case of uncapped Ge NCs with the increasing of Si capping shells.

4 Summary and Conclusions

By means of an *ab initio* pseudopotential method based on density-functional theory we investigated large semiconductor nanocrystallites concerning their structural, electronic and optical properties, when they are oxidized, capped, and doped with impurities of the groups III, IV, and V. The overall effect of capping with oxide shells in Si NCs is to narrow the HOMO-LUMO gap and expand the Si-Si bonds at the core of the NC, in particular when the Si NCs are oxidized via passivation with OH. Oxygen-related defects in oxidized Si NCs may have influence on the spatial distribution of the HOMO and LUMO, though their influence on the electronic properties is small. Capping of Si NCs with Ge shells apparently leads to more strain than the capping of Ge NCs with Si shells. The onsets

of absorption of Si (Ge) NCs capped with Ge (Si) shells shifts due to the contribution of quantum confinement effects and overall composition of the capped NC. Except for Ge, the formation energy of an impurity in doped Si nanocrystallites tends to be higher than in bulk Si. The impurity formation energies depend significantly on the shape of the Si NCs. As for bulk Si, B and Al introduce shallow acceptor levels and N and P introduce donor levels in Si NCs. There is less dependence of the impurity energy levels with respect to the shape of the Si NCs. Doping with C may narrow the HOMO-LUMO gap, whereas doping with Ge practically does not change the gap. Our results help to clarify some aspects of electronic structure and optical spectra of semiconductor nanocrystallites.

References

1. A.G. Cullis, L.T. Canham, and P.D.J. Calcott, *The structural and luminescence properties of porous silicon*, J. Appl. Phys. **82**, 909–965, 1997.
2. O. Bisi, S. Ossicini, and L. Pavesi, *Porous silicon: a quantum sponge structure for silicon based optoelectronics*, Surf. Sci. Rep. **38**, 1–126, 2000.
3. L. Pavesi, L. Dal Negro, C. Mazzoleni, G. Franzò, and F. Priolo, *Optical gain in silicon nanocrystals*, Nature (London) **408**, 440–444, 2000.
4. J. Linnros, *Nanocrystals brighten transistors*, Nature Materials (London) **4**, 117–119, 2005.
5. M.V. Wolkin, J. Jorne, P.M. Fauchet, G. Allan, and C. Delerue, *Electronic States and Luminescence in Porous Silicon Quantum Dots: The Role of Oxygen*, Phys. Rev. Lett. **82**, 197–200, 1999.
6. L.E. Ramos, J. Furthmüller, and F. Bechstedt, *Reduced influence of defects on oxidized Si nanocrystallites*, Phys. Rev. B **71**, 035328-1–035328-7, 2005.
7. L.E. Ramos, J. Furthmüller, and F. Bechstedt, *Effect of backbond oxidation on silicon nanocrystallites*, Phys. Rev. B **70**, 033311-1–033311-4, 2004.
8. L.E. Ramos, J. Furthmüller, and F. Bechstedt, *Influence of Oxygen on Optical Properties of Si Nanocrystallites*, Appl. Phys. Lett. **87**, 143113-1–143113-3, 2005.
9. L.E. Ramos, J. Furthmüller, and F. Bechstedt, *Quantum confinement in Si- and Ge-capped nanocrystallites*, Phys. Rev. B **72**, 045351-1–045351-8, 2005.
10. L.E. Ramos, E. Degoli, G. Cantele, S. Ossicini, D. Ninno, J. Furthmüller, and F. Bechstedt, *Structural features and electronic properties of group-III, group-IV, and group-V doped Si nanocrystallites*, J. Phys. C: Condens. Matter. **19**, 466211-1–466211-12, 2007.
11. G. Kresse and J. Furthmüller, *Efficiency of ab-initio total energy calculations for metals and semiconductors using a plane-wave basis set*, Comput. Mater. Sci. **6**, 15–50, 1996.
12. G. Kresse and J. Furthmüller, *Efficient iterative schemes for ab initio total-energy calculation using a plane-wave basis set*, Phys. Rev. B **54**, 11169–11186, 1996 .
13. G. Kresse and D. Joubert, *From ultrasoft pseudopotentials to the projector augmented-wave method*, Phys. Rev. B **59**, 1758–1775, 1999 .
14. `http://cms.mpi.univie.ac.at/vasp/`.
15. `http://www.netlib.org`.
16. `http://math-atlas.sourceforge.net`.